Supplementary Materials

A hole-transport material that also passivates perovskite surface defects for solar cells with improved efficiency and stability

*By Xiaoming Zhao[1], Chao Yao[1,#], Kaichen Gu[1], Tianran Liu[1], Yu Xia[1] and Yueh-Lin Loo[1,2,]**

[1] Department of Chemical and Biological Engineering, Princeton University, Princeton, New Jersey 08544, United States.

[2] Andlinger Center for Energy and the Environment, Princeton University, Princeton, New Jersey 08544, United States.

* Corresponding author: Yueh-Lin Loo (Email: lloo@princeton.edu)

[#] Present address: School of Advanced Materials, Peking University Shenzhen Graduate School, Shenzhen, 518055 China.

Experimental Section

Materials: PbI_2 (99.99%) was purchased from TCI America. MAI (>99%), FAI (>99%) and TiO_2 paste (30 NR-D) were purchased from Greatcell Solar. CsI (99.5%) was purchased from Sigma Aldrich. MACl (>99%) was purchased from Yingkou Libra Technology. DMF (>99.8%), DMSO (>99.8%), chlorobenzene (>99.8%), chloroform (>99.8%) and diethyl ether (>99.8%) were purchased from Acros Organics. Acetylacetone (>99%), titanium diisopropoxide (75 wt. % in isopropanol), Spiro-OMeTAD (>99%), Li-TFSI (99.95%), t-BP (98%) were purchased from Sigma Aldrich. Acetone, IPA and other solvents were purchased from Fisher Scientific. All chemicals were used as-received without further purification. Solar cell substrates are pre-patterned fluorine-doped tin-oxide-coated (FTO) glass (<15 Ω /square) obtained from Yingkou Advanced Election Technology Co., Ltd.

Synthesis of YZ18 and YZ22:

YZ18

2,7-dibromophenanthrene (1 mmol, 0.333 g), (4-(bis(4-methoxyphenyl)amino)phenyl)boronic acid (2.5 mmol, 0.875 g), toluene (10 mL), ethanol (2 mL) and aqueous potassium carbonate (2.5 mL, 1 M) were added to a 25 mL three-necked flask. The mixture was purged using nitrogen for 15 min and then $Pd(PPh_3)_4$ (50 mg) was added. After heating at 90 ℃ for 24 h, the mixture was cooled down to room temperature. 20 mL dichloromethane was added to fully dissolve the product compound. The organic layer was washed by water for three times and then was dried with anhydrous Na_2SO_4. Solvent was removed by rotary evaporator and crude product was obtained. Further purification was carried out by column chromatography (petroleum ether: dichloromethane = 1:10) and YZ18 was obtained as light yellow solid (0.541 g, 69% yield). YZ18 can also be recrystallized from a mixture of methanol and dichloromethane (1:3 in volume). ^{1}H NMR (500 MHz, $CDCl_3$) δ: 8.70-8.72(d, 2H), 8.06(s, 2H) 7.89-7.91(d, 2H), 7.80(s, 2H), 7.61-7.63(d, 4H), 7.13-7.28(d, 8H), 7.07-7.09(d, 4H), 6.87-6.90(d, 8H), 3.84(s, 12H). ^{13}C NMR (126 MHz, $CDCl_3$) δ: 155.93, 148.31, 140.87, 138.70, 132.56, 132.35, 128.84, 127.72, 127.45, 126.67, 126.41, 125.63, 125.47, 123.13, 120.82, 114.74, 114.64, 55.53. MS (m/z): calculated 784.33, found 784.09.

YZ22

3,8-dibromo-1,10-phenanthroline (1 mmol, 0.338 g), (4-(bis(4-methoxyphenyl)amino)phenyl)boronic acid (2.5 mmol, 0.875 g), toluene (10 mL), ethanol (2 mL)

and aqueous potassium carbonate (2.5 mL, 1 M) were added to a 25 mL three-necked flask. The mixture was purged using nitrogen for 15 min and then $Pd(PPh_3)_4$ (50 mg) was added. After heating at 90 ℃ for 24 h, the mixture was cooled down to room temperature. 30 mL dichloromethane was added to fully dissolve the product compound. The organic layer was washed by water for three times and then was dried with anhydrous Na_2SO_4. Solvent was removed by rotary evaporator and crude product was obtained. Further purification was carried out by column chromatography (we first used triethylamine to neutralize the silica gel and then used petroleum ether: dichloromethane = 1:1 as the column chromatography solvents) and YZ22 was obtained as an orange solid (0.572 g, 74% yield). YZ22 can also be recrystallized from a mixture of methanol and dichloromethane (1:3 in volume). ^{1}H NMR (500 MHz, $CDCl_3$) δ: 9.41-9.42(s, 2H), 8.33(s, 2H), 7.85(s, 2H),7.62-7.64(d, 4H), 7.15-7.16(d, 8H), 7.09-7.10(d, 4H), 6.89-6.91(d, 8H), 3.84(s, 12H). ^{13}C NMR (126 MHz, $CDCl_3$) δ: 156.21, 149.23, 149.14, 144.60, 140.48, 135.22, 132.05, 128.90, 128.40, 127.96, 127.00, 126.95, 120.46, 114.83, 55.54, 46.24. MS (m/z): calculated 786.32, found 786.02.

Synthesis of perovskite single crystals: $FAPbI_3$ and $MAPbI_3$ crystals were synthesized following the literature.[1] $CsPbI_3$ crystals were synthesized following the literature.[2]

Perovskite precursor solutions and spin-coating procedures

Perovskite precursor solutions were prepared in a nitrogen-filled glovebox.

$\underline{MAPbI_3}$

Pre-synthesized $MAPbI_3$ single crystals were dissolved in a mixed solvent of DMF and DMSO (9:1 v/v) to make a 1.45 M precursor solution. Perovskite thin films were prepared by spin-coating the precursor solution at 1000 rpm for 10 s and 6000 rpm for 30 s, with an acceleration rate of 200 and 2000 rpm/s, respectively. 19 s before the end, 200 μL of chlorobenzene was dripping onto the substrate. The films were then thermally annealed at 100 ℃ for 1 hour to remove residual solvent.

$\underline{Cs_{0.1}FA_{0.9}PbI_3}$

Pre-synthesized $FAPbI_3$ and $CsPbI_3$ crystals (molar ration = 9:1) with addition of 20 mol% MACl additives were dissolved in a mixed solvent of DMF and DMSO (9:1 v/v) to make a 1.40 M precursor solution. Perovskite thin films were prepared by spin-coating the precursor solution at 1000 rpm for 5 s and 5000 rpm for 20 s, with an acceleration rate of 200 and 2000 rpm/s, respectively. 10 s before the end, 1 mL of diethyl ether was dripping onto the substrate. The films were then thermally annealed at 150 ℃ for 10 min and then at 100 ℃ for 30 min.

Device Fabrication. Perovskite solar cells were fabricated on pre-patterned FTO glass substrates. The substrates were cleaned with deionized water, acetone, isopropanol and UV-Ozone cleaner, each step taking 15 minutes. A compact titanium dioxide (TiO_2) layer of about 40 nm was deposited by spray pyrolysis of 7 mL 2-propanol solution containing 0.6 mL titanium diisopropoxide bis(acetylacetonate) solution and 0.4 mL acetylacetone at 450 °C using oxygen as the carrier gas. On top of this layer, about 150 nm of mesoporous TiO_2 layer was formed by spin-coating TiO_2 paste diluted in ethanol (1:5.5 w/w) at 4500 rpm for 20 s and then the stack was sintered at 500 °C for 30 minutes. The active layer was deposited by spin-coating, with the same conditions that were used to prepare the perovskite films. Subsequently, the hole-transport layer was deposited on top of the active layer by spin-coating HTM solution at 4000 rpm for 20 s. The YZ18 and YZ22 solutions were prepared by dissolving YZ18 or YZ22 in chloroform at a concentration of 40 mM. Doped Spiro-OMeTAD solutions were prepared by dissolving the Spiro-OMeTAD in 1 mL chlorobenzene at a concentration of 60 mM, with the addition of 30 mM Li-TFSI from a stock solution in acetonitrile and 200 mM of *t*-BP. Finally, the devices were completed by thermal evaporation of 100-nm thick gold as top contacts. The active area (0.16 cm^2) was determined using a shadow mask.

Characterizations: UV-vis absorption spectra were obtained on an Agilent Technologies Cary 5000 spectrophotometer. Steady-state PL and time-resolved PL were measured with an Edinburgh Instruments FLS980 photoluminescence spectrometer. Time-resolved PL were measured with excitation and detection wavelength being 526 nm and 800 nm, respectively; The pulsed excitation fluence is 4.2 nJ cm^{-2}. Steady-state PL were measured with an excitation wavelength of 520 nm and powder density of 1mW cm^{-2}. GIWAXS measurements were performed at the Complex Materials Scattering (CMS) beamline of the National Synchrotron Light Source II (NSLS-II), Brookhaven National Lab. The X-ray beam has an energy of 13.5 eV and the thin film samples were placed 257 mm away from the detector. XRD measurements were conducted on a Bruker D8 Discover diffractometer using Cu Kα radiation source (λ = 1.54 Å). The step size was 0.01°. Mass spectra were recorded on a FINNIGAN LCQ Advantage mass spectrometer. Differential scanning calorimetry (DSC) was conducted on TA Q20 Instrument. ^{1}H- and ^{13}C-NMR spectra were measured with Bruker AVANCE 500 MHz NMR spectrometer. Film thickness were determined by Bruker Dimension ICON3 Atomic Force Microscope. UPS measurements were performed with a ThermoFisher Ultraviolet + X-ray Photoelectron Spectrometer using the He I (21.2 eV)

discharging lamp. The Fermi edge of a gold film was used to calibrate the E_F position. XPS measurements were performed with a ThermoFisher Ultraviolet + X-ray Photoelectron Spectrometer using a monochromatic Al K_α X-ray of 24.8 W power. Core-level signals were obtained at 45° take-off angle. All peaks were calibrated using C 1s peak at 284.8 eV to correct shift of binding energies. Curve fitting was performed using the PHI MultiPak software. Depth profiling etching speed was calibrated using Si as standard. ATR-FTIR spectra were measured with a Thermo Scientific Nicolet iN10 MX infrared imaging microscope. A low-voltage scanning electron microscope (FEI Verios 460 XHR) was used to record SEM images. The accelerating voltage was kept at 3 keV to prevent beam damage to the specimens.

Solar Cell Characterization. The current density-voltage (*J-V*) characteristics of the photovoltaic devices were measured using a Keithley 2635 source-measurement unit. A solar simulator with Xenon lamp (300 W) and an AM 1.5G filter were used as the solar simulator. A Newport reference cell (model 71582) was used for calibration. To calibrate the light intensity of the solar simulator (100 mW cm^{-2}), the power of the Xenon lamp was adjusted to match the short-circuit current density (J_{SC}) of the reference cell under simulated sunlight to that specified by the manufacturer. A light aperture with the same size as the active area (0.16 cm^2; the light aperture is the same one as the shadow mask for electrodes evaporation) was used to shadow the devices. External quantum efficiency measurements were performed using a 300 W Xenon arc lamp (Newport Oriel), with filtered monochromatic light from a Cornerstone 260 1/4 M double-grating monochromator (Newport 74125). A silicon photodiode (model 71580) calibrated at Newport was used as the reference cell. The step size for EQE measurement is 1 nm. The *J-V* measurements of all devices were performed on unencapsulated cells in ambient environment without any preconditioning. The scan speed and dwell time were 0.01 V s^{-1} and 0.05 s (reverse scan: 1.2 to -0.2 V, forward scan: -0.2 to 1.2 V), respectively.

Mobility Measurement: Hole-only devices (Au/HTL/Au) were fabricated to extract the hole mobility of HTMs. The dark *J-V* characteristics of the hole-only devices were measured by a Keithley 2635 source-measurement unit.

Encapsulation and stability measurement under continuous illumination: Devices were encapsulated in a nitrogen glovebox using a cover glass with an attachment of Dynic HG Sheet Desiccant (SF type, 100 μm thick) and a UV-curable epoxy (Epoxy Technology, OG159-2) applied along its perimeter. The stability study on devices was conducted according to the ISOS-L-

1I protocol.[3] Encapsulated devices were mounted on homebuilt printed circuit boards and connected to a Keithley 2401 and a Keithley 2700 with two 7705 multiplexer units. Devices were aged under continuous illumination from a Philips metal-halide lamp with a power density of 1.1 sun (Philips MSR 1200 HR). The lamp spectrum was monitored by an Ocean Optics spectrometer throughout the entire aging test and no significant changes in the spectrum were observed. For room-temperature stability studies, a liquid cold plate was used to hold the packaged devices and the temperature of the cold plate was maintained at 30 ± 2 °C for the duration of the experiment. For thermal stability studies, the cells were placed on a hotplate with temperature of 85 ℃. The current density versus voltage (*J-V*) characteristics were measured every 6 minutes. The initial values at the maximum power point (MPP) were obtained from each *J-V* sweep, and then devices were kept at the MPP during operation by an active load system developed by infinityPV ApS.

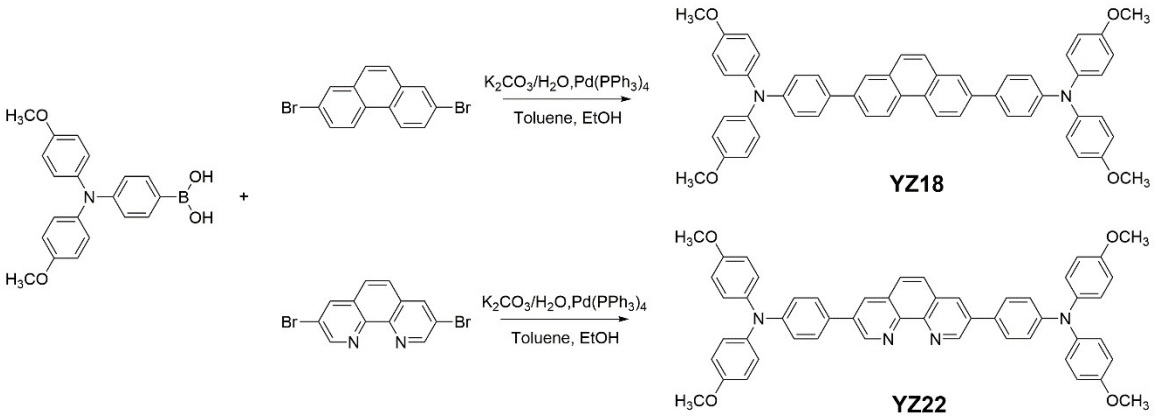

Figure S1. Synthetic routes to YZ18 and YZ22.

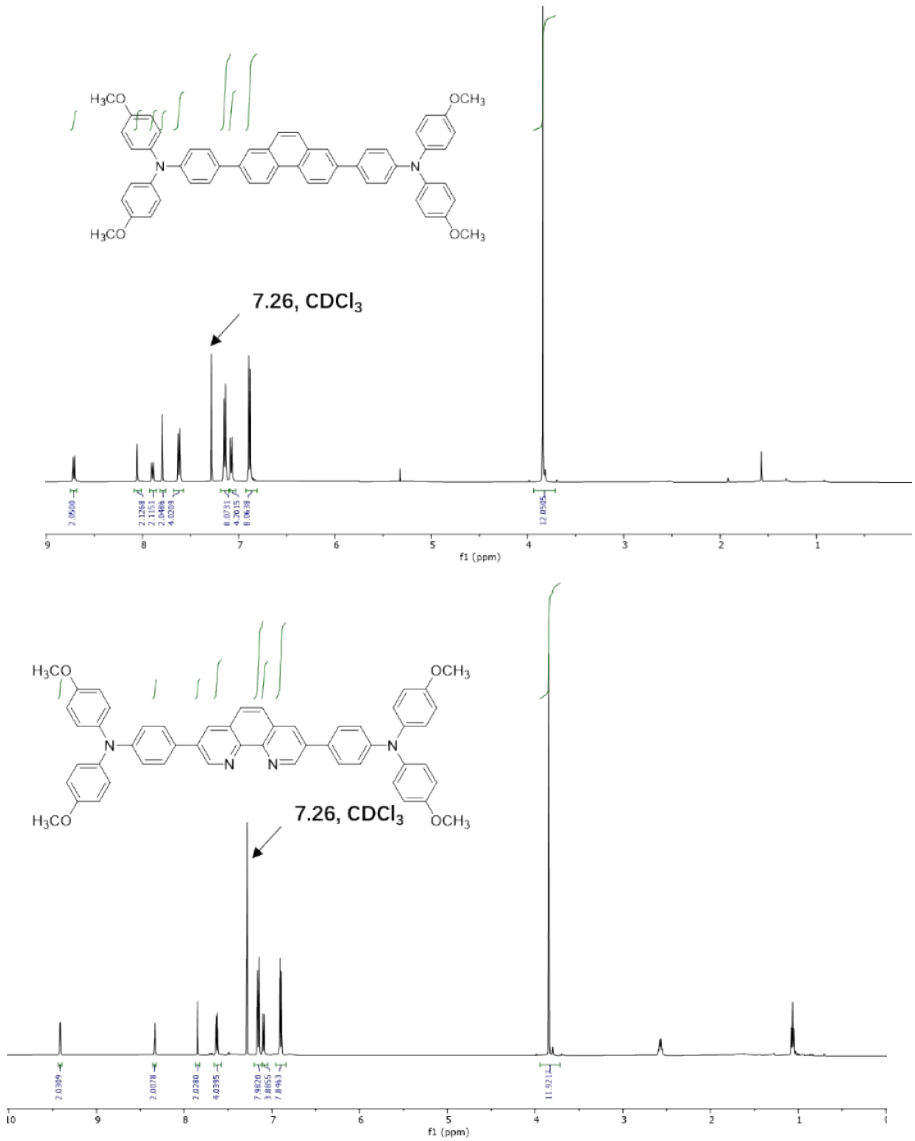

Figure S2. ^{1}H NMR spectra of YZ18 and YZ22 with $CDCl_3$ as the solvent.

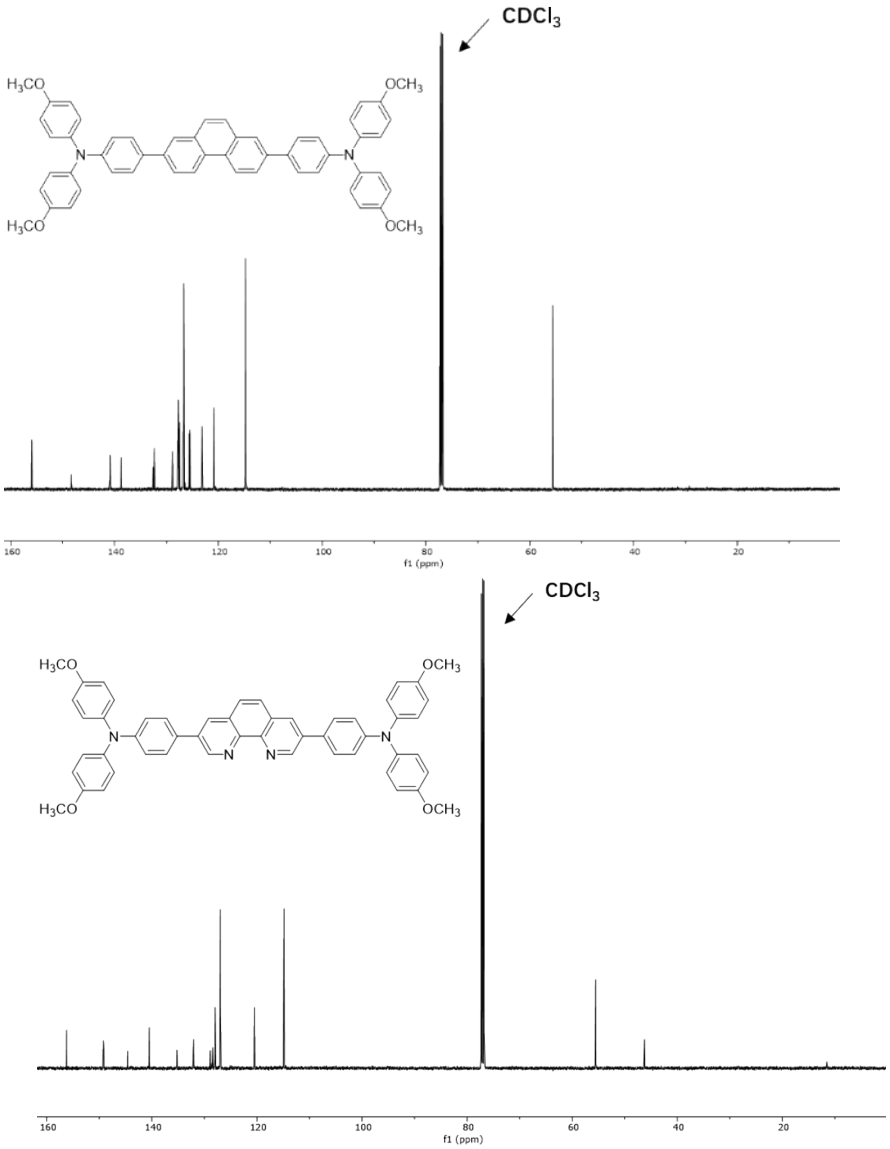

Figure S3. ^{13}C NMR spectra of YZ18 and YZ22 with $CDCl_3$ as the solvent.

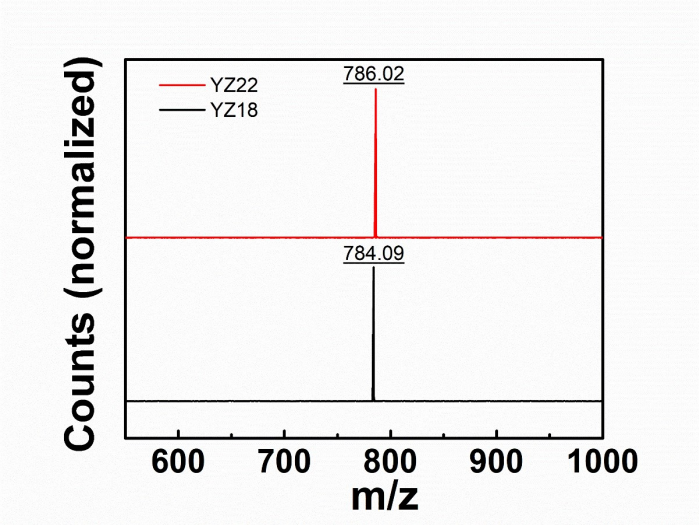

Figure S4 Mass spectra of YZ18 and YZ22.

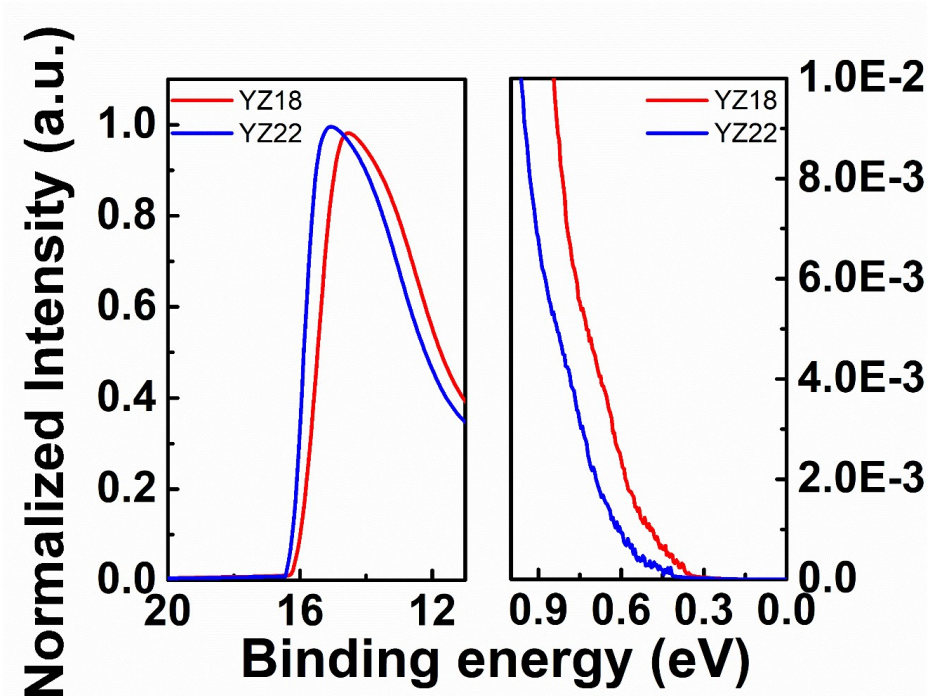

Figure S5. UPS spectra of YZ18 and YZ22 in (left) secondary electron cut-off region and (right) valence band region.

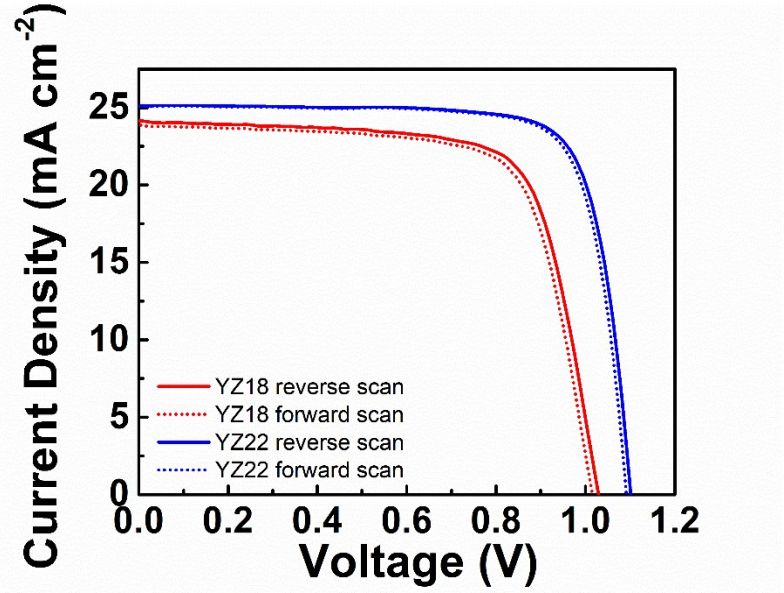

Figure S6. *J–V* characteristics of CsFAPbI-based PSCs under both forward and reverse scan directions with either YZ18 or YZ22 as HTM.

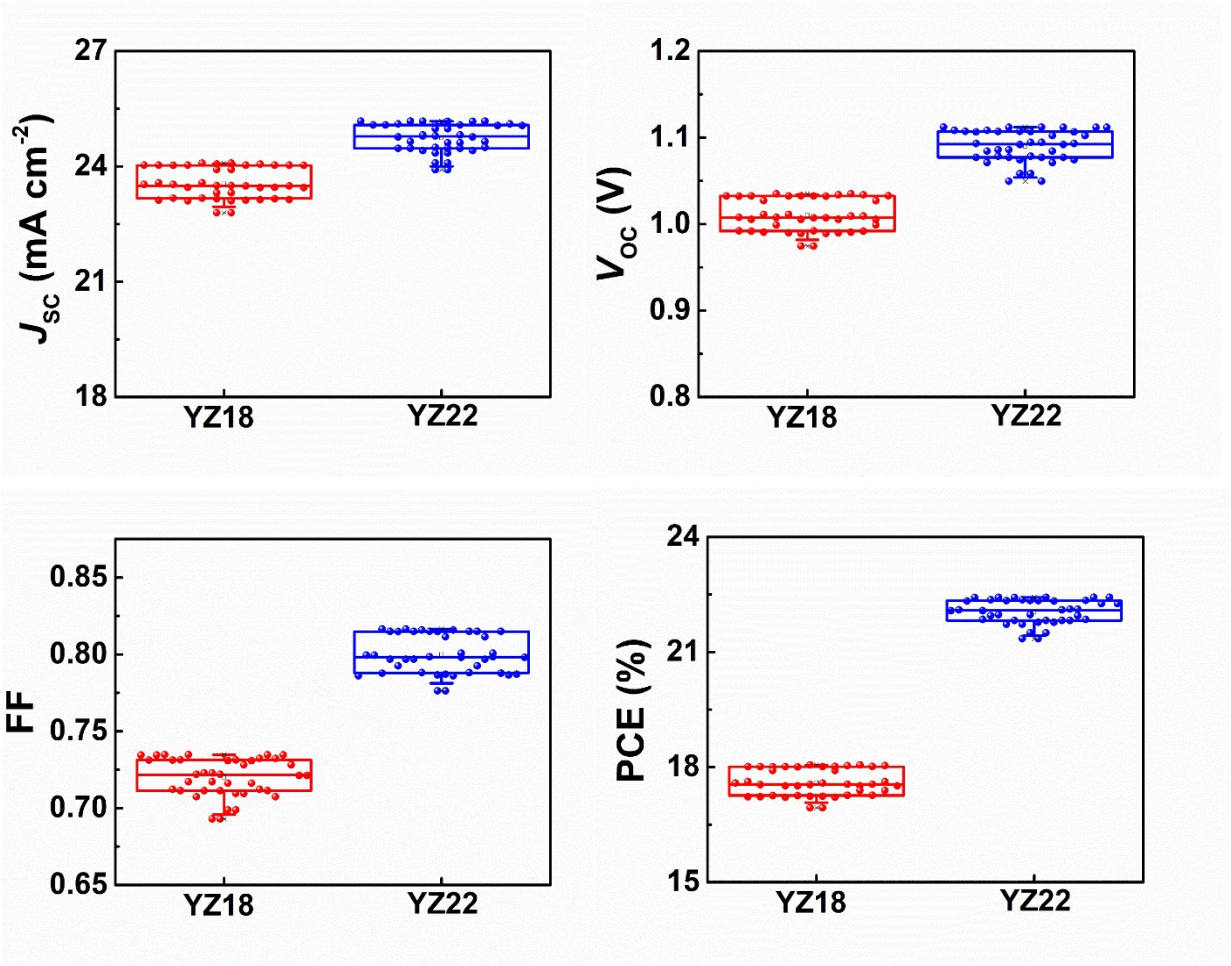

Figure S7. Solar-cell performance statistics of CsFAPbI PSCs with either YZ18 or YZ22 as HTM. Values were extracted from testing 40 devices at each condition.

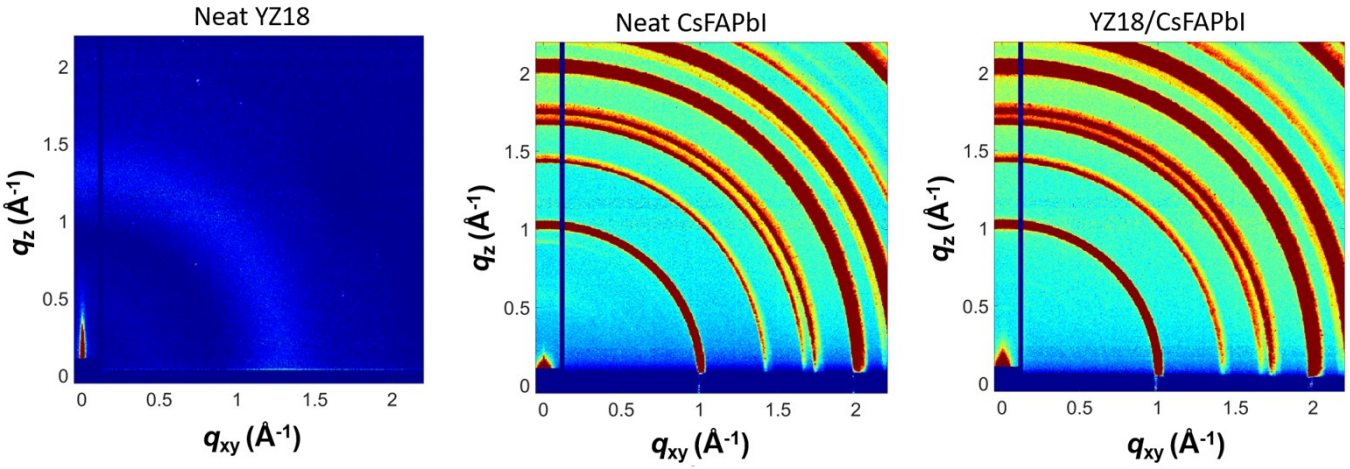

Figure S8. GIWAXS patterns of YZ18, CsFAPbI, and a stack comprising YZ18 on CsFAPbI. The incident angle during data acquisition is 0.1°.

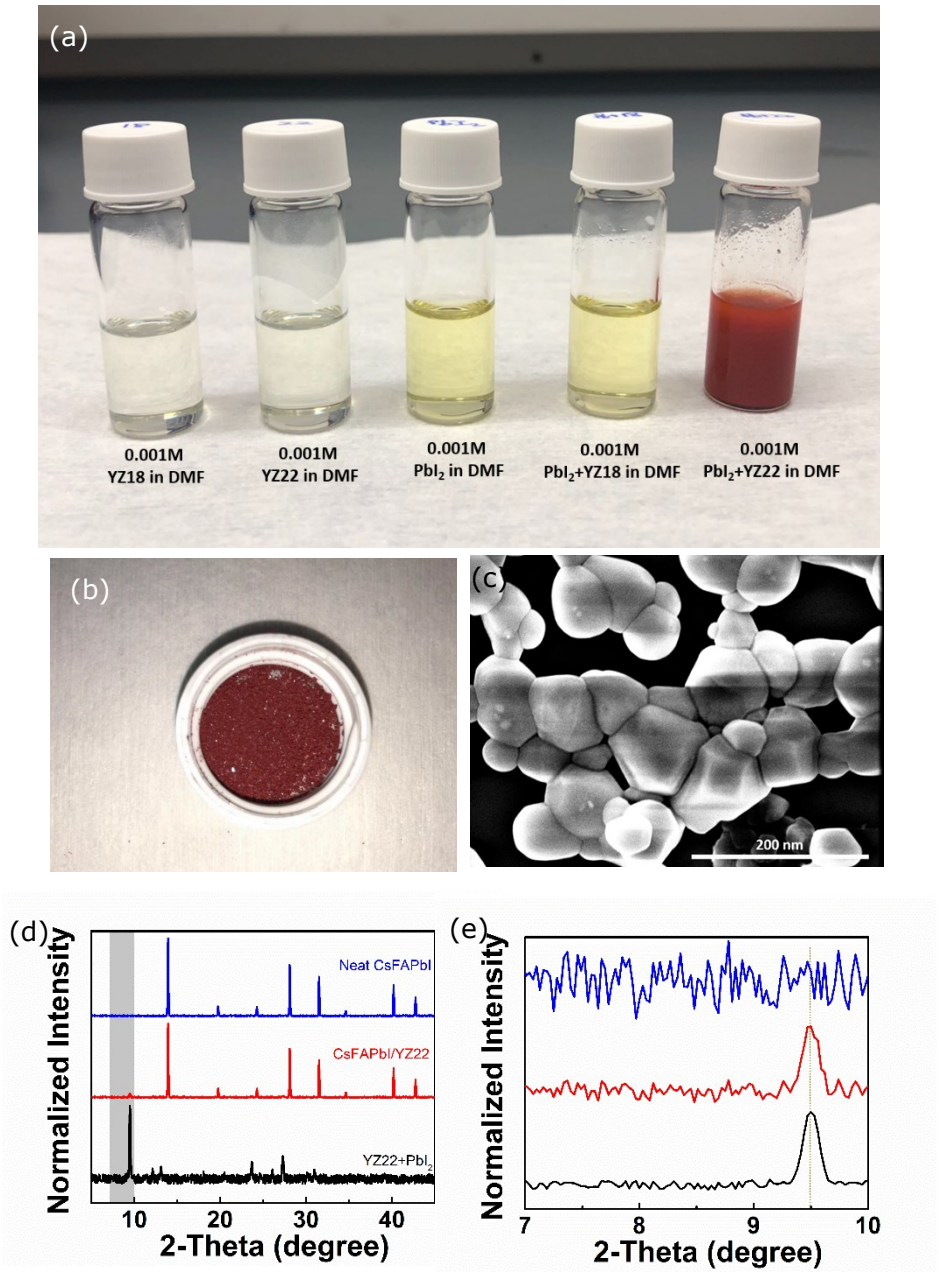

Figure S9 (a) Photographs of solutions showing complexation and precipitation when PbI_2 and YZ22 are mixed in DMF; (b) Photograph and (c) SEM images of (YZ22+PbI_2) precipitate; (d-e) XRD traces of CsFAPbI, CsFAPbI/YZ22 and the fine powder obtained when PbI_2 and YZ22 are mixed in DMF. The grey portion of the traces are magnified in (e) to reveal evidence for the complexation between PbI_2 and YZ22.

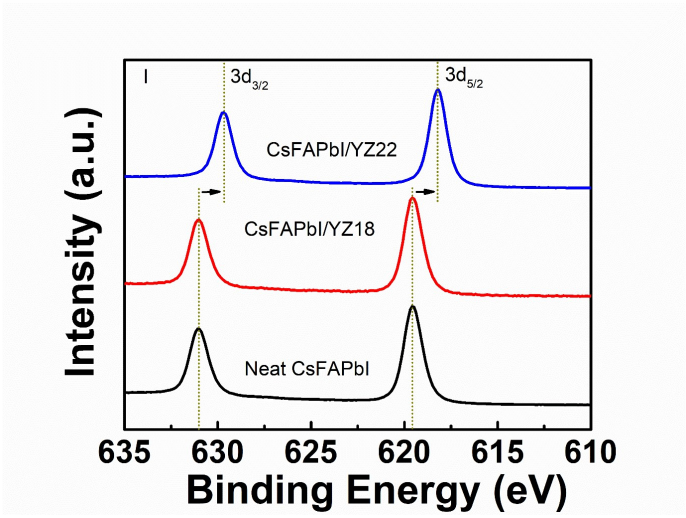

Figure S10 XPS spectrum of I 3d of CsFAPbI, of a stack comprising YZ18 on CsFAPbI, and of a stack comprising YZ22 on CsFAPbI.

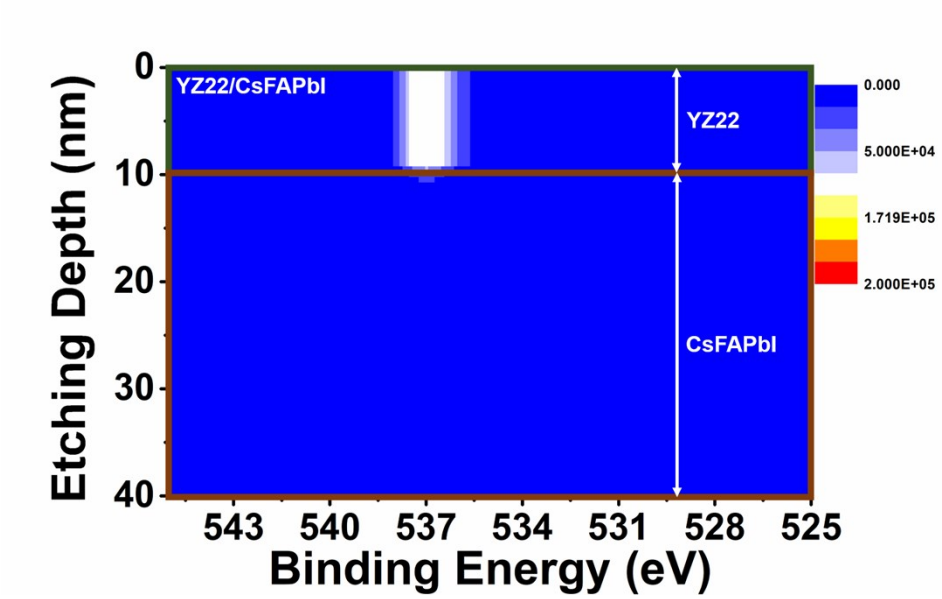

Figure S11. XPS O1s depth filing of a stack comprising 10 nm of YZ22 on CsFAPbI.

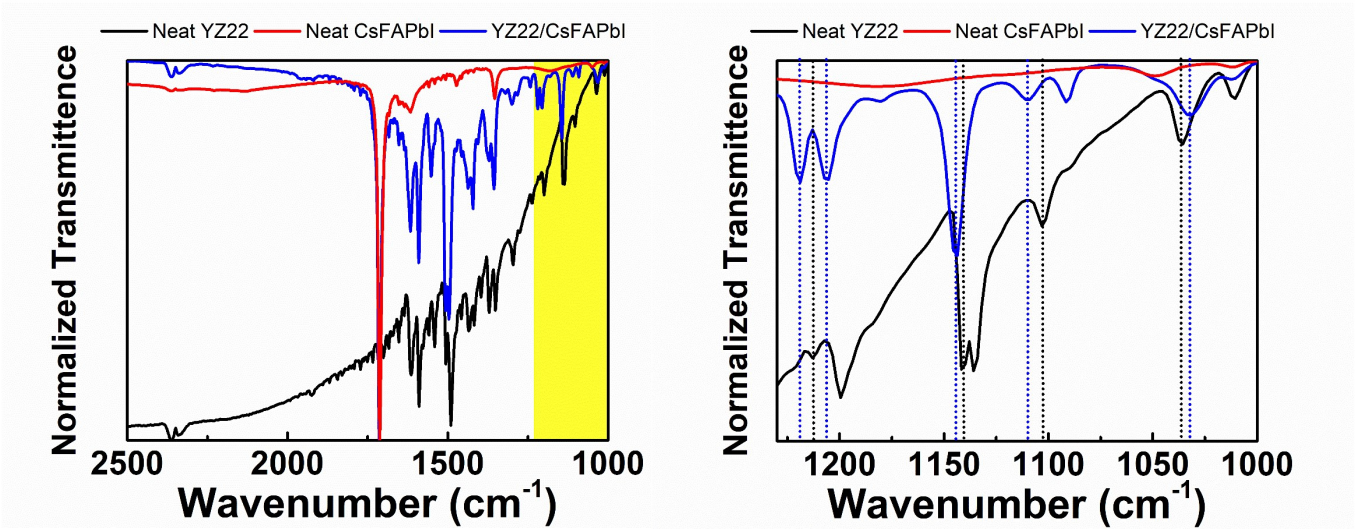

Figure S12. FTIR spectra of YZ22, CsFAPbI, and of a stack comprising YZ22 on CsFAPbI. The region highlighted in yellow is magnified in the right panel.

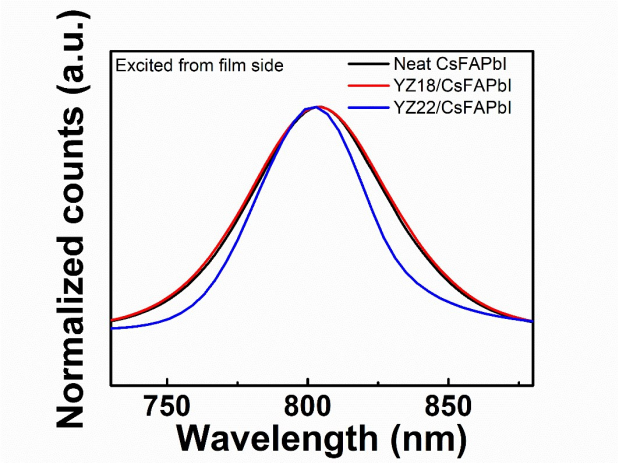

Figure S13. Normalized steady-state PL spectra of CsFAPbI, stacks comprising YZ18 on CsFAPbI and YZ22 on CsFAPbI excited from the film side.

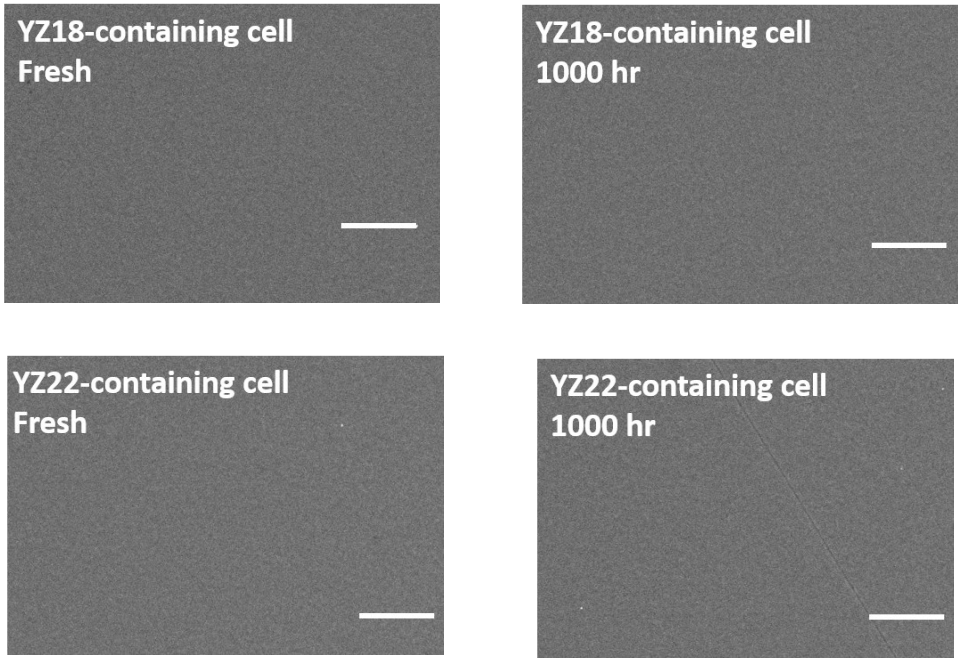

Figure S14 Top-view SEM images of the surface of FTO/TiO_2/CsFAPbI/HTL (YZ22 or YZ18) stacks before and after device stability studies. The scale bar is 5 μm. To obtain SEM images of devices after aging, we mechanically removed the cover slides that once encapsulated the devices, and then used Scotch tape to peel off the Au electrodes, following the method suggested in the literature.[4]

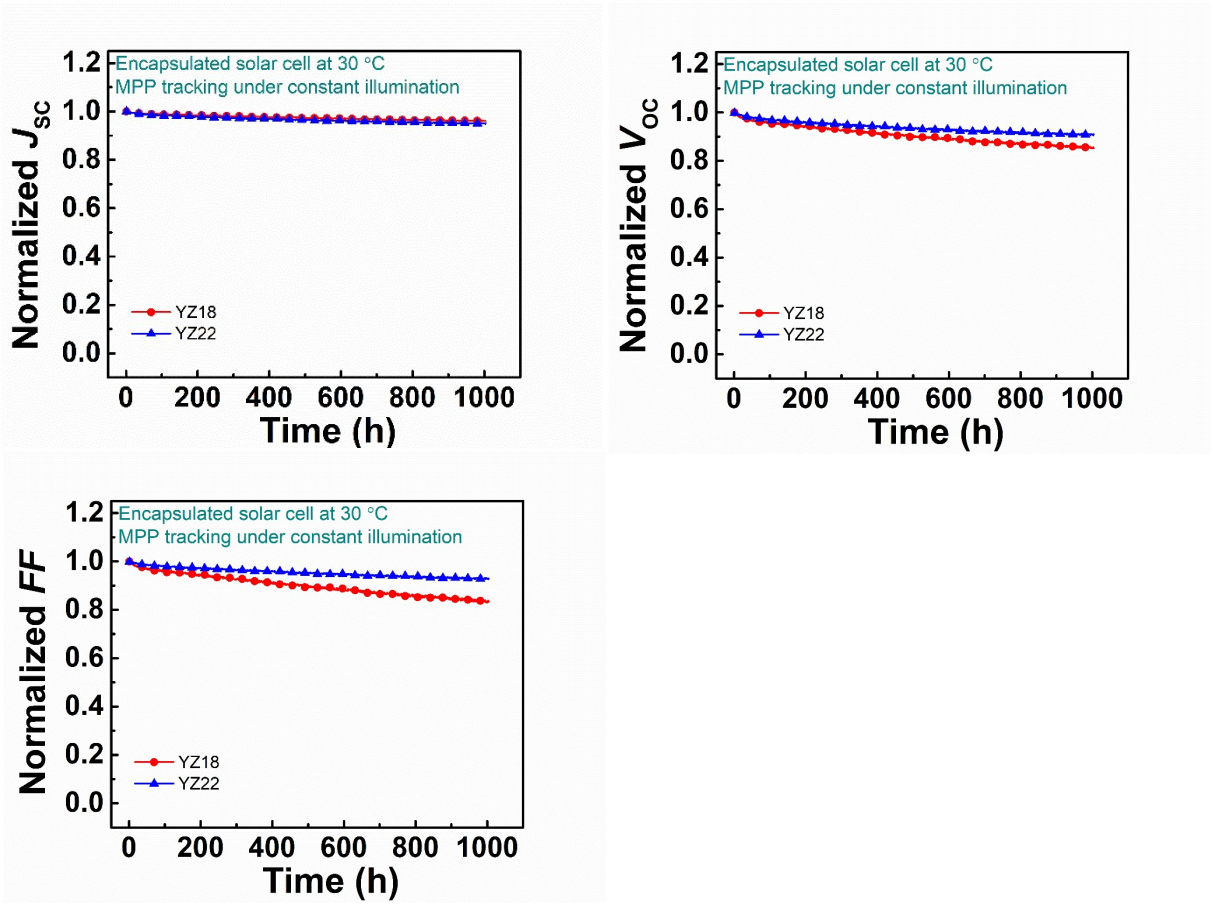

Figure S15. Normalized photovoltaic parameters over time for encapsulated CsFAPbI devices with YZ18 or YZ22 as HTL that were held at MPP at 30 °C under an equivalent of ~1.1 sun illumination. Data points are averaged values obtained from 5 devices studied under each condition

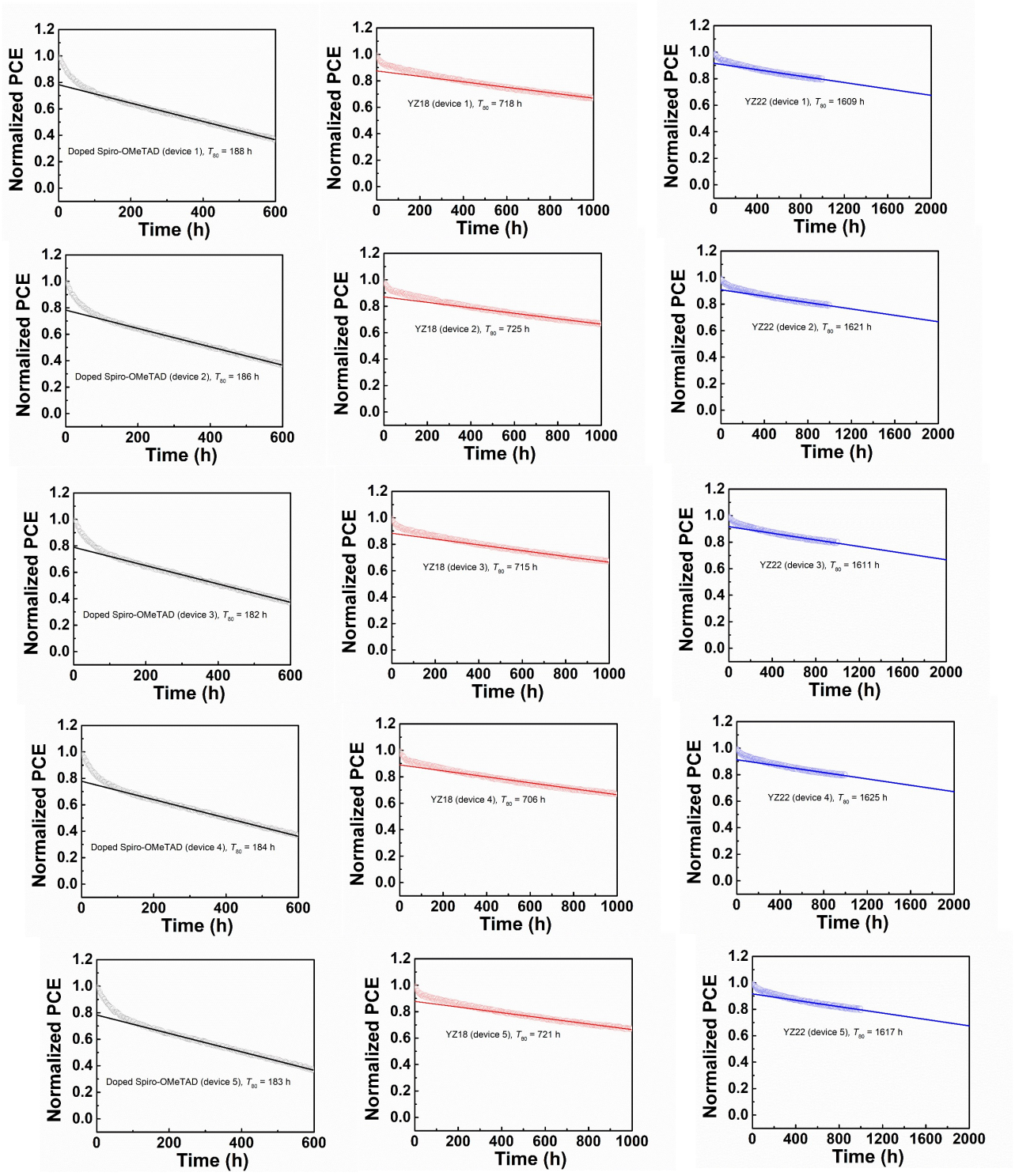

Figure S16. Estimation of T_{80} values for encapsulated CsFAPbI devices with doped Spiro-OMeTAD, YZ18 or YZ22 as HTL that were held at MPP at 30 °C under an equivalent of ~1.1 sun illumination. We followed the reported method of Snaith et al. to estimate T_{80} to quantify the lifetimes of these CsFAPbI solar cells.[5] For devices that exhibit 'burn-in', we fitted the stability

data after the initial decay associated with burn-in to a straight line, and extrapolated the curve back to time zero to obtain the $T = 0$ efficiency. We then determined the lifetime at 80% of the $T = 0$ efficiency.

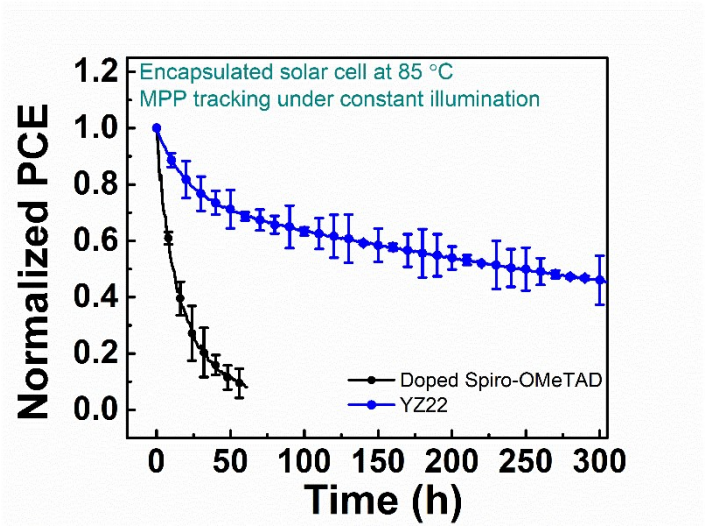

Figure S17 Normalized PCE over time for encapsulated CsFAPbI devices with doped Spiro-OMeTAD or dopant-free YZ22 as HTL that were hold at MPP at 85 °C in air under a constant 1.1-sun illumination. Average values and standard deviations were obtained from 5 devices studied under each condition.

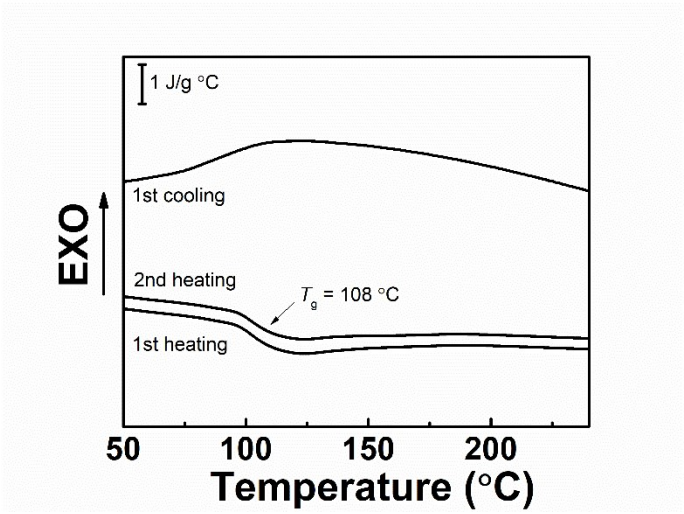

Figure S18 Differential scanning calorimetry heating and cooling curves of YZ22 (heating and cooling rate: 10 K min^{-1} in N_2 atmosphere).

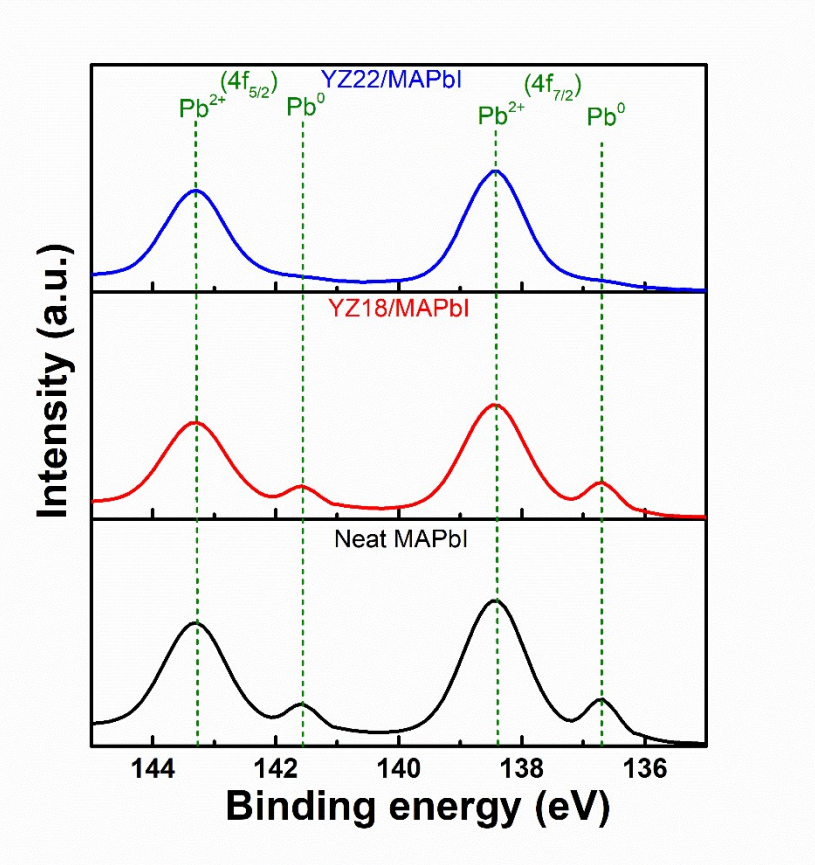

Figure S19. XPS of Pb 4f core level of MAPbI film, a stack comprising 10 nm of YZ18 on MAPbI and a stack of 10 nm of YZ22 on MAPbI. The XPS traces for the stacks were obtained at a depth of 10 nm from the surface.

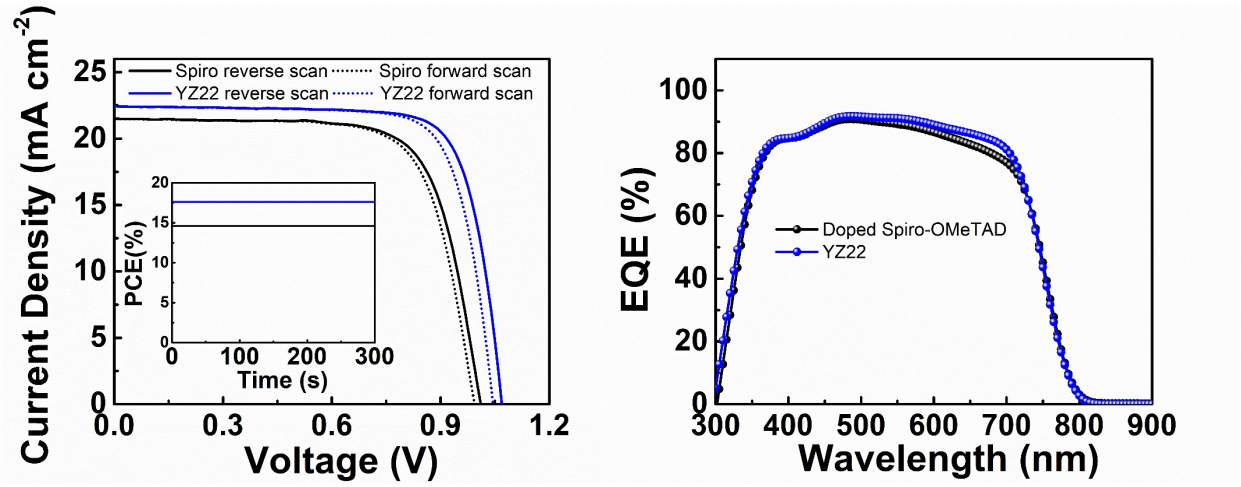

Figure S20. *J–V* characteristics, stabilized output and EQE of MAPbI-based PSCs with either doped Spiro-OMeTAD or YZ22 as HTM. Note: "Spiro" is short for doped Spiro-OMeTAD in these figures.

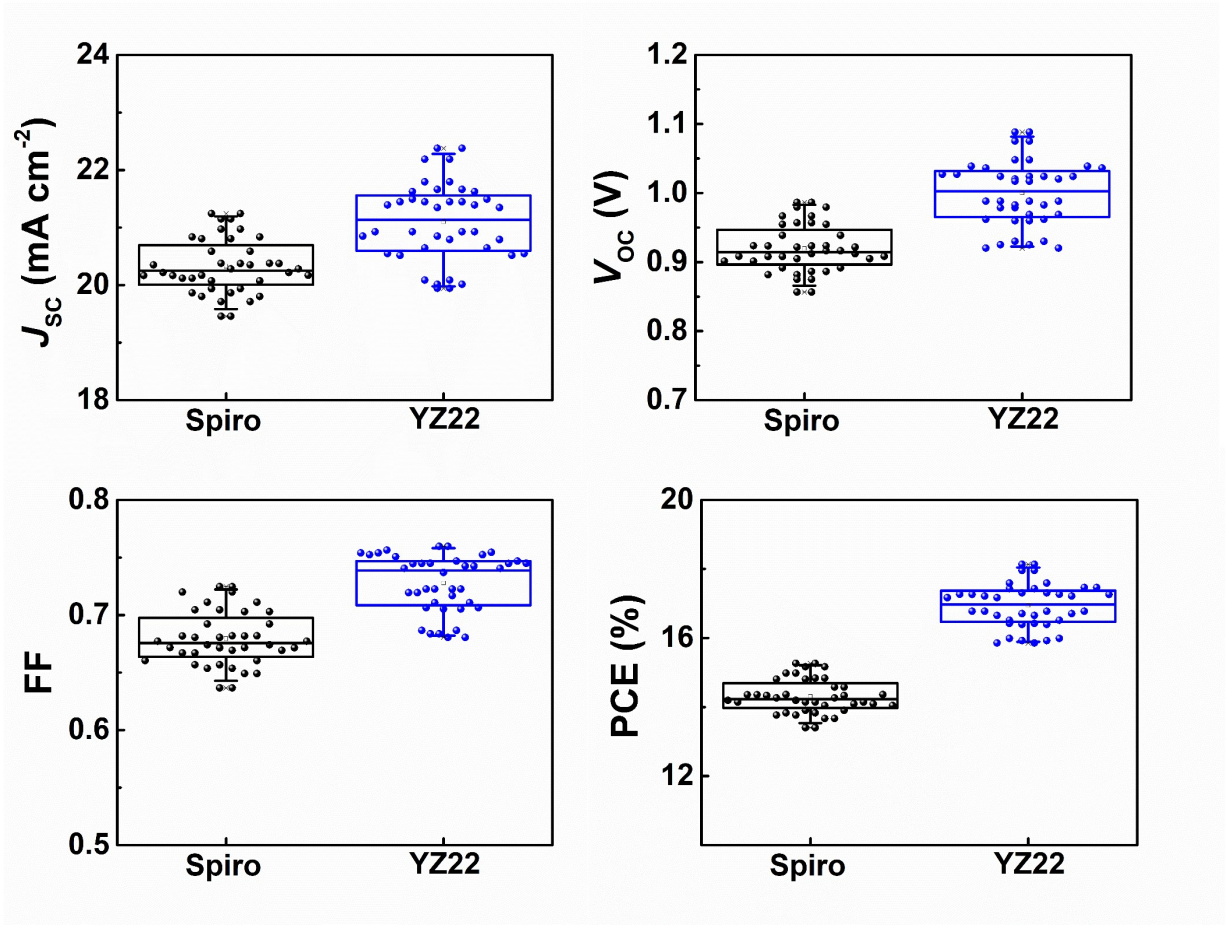

Figure S21. Solar-cell performance statistics of MAPbI PSCs with either doped Spiro-OMeTAD or YZ22 as HTM. Values were extracted from testing 40 devices at each condition. Note: "Spiro" is short for doped Spiro-OMeTAD in these figures.

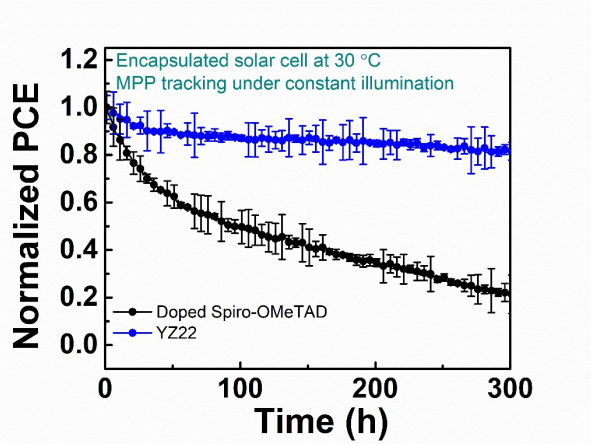

Figure S22. Normalized PCE as a function of operation time of encapsulated MAPbI solar cells at 30℃ in air under continuous illumination (1.1-sun) at MPP with either doped Spiro-OMeTAD or YZ22 as HTL. Average values and standard deviations were obtained from 5 devices studied under each condition.

Table S1. Summary of performance of representative PSCs with dopant-free small-molecular HTMs.

HTM	Device configuration (ETL/Perovskite/HTL)	PCE (%)	Ref.
BTF4	SnO_2+PCBM/$(FAPbI_3)_{0.85}(MAPbBr_3)_{0.15}$/HTM	18.0	[6]
YN2	TiO_2/$(FAPbI_3)_{0.85}(MAPbBr3)_{0.15}$/HTM	19.2	[7]
PYR16	TiO_2/ $Cs_{0.05}(MA_{0.17}FA_{0.83})_{0.95}Pb(I_{0.83}Br_{0.17})_3$/HTM	17.0	[8]
DTPC13-ThTPA	SnO_2+C_{60}/$MA_{0.7}FA_{0.3}PbI_{2.85}Br_{0.15}$/HTM	20.3	[9]
DTP-C6Th	SnO_2+C_{60}/$MA_{0.7}FA_{0.3}Pb(I_{0.925}Br_{0.075})_3$/HTM	21.0	[10]
FA-CN	TiO_2/$(FAPbI_3)_{0.85}(MAPbBr_3)_{0.15}$/HTM	18.9	[11]
TTE-2	SnO_2/$(FAPbI_3)_{0.95}(MAPbBr_3)_{0.05}$/HTM	20.0	[12]
YZ18	**TiO_2/$Cs_{0.1}FA_{0.9}PbI_3$/HTM**	**18.1**	**This work**
YZ22	**TiO_2/$Cs_{0.1}FA_{0.9}PbI_3$/HTM**	**22.4**	**This work**

Table S2. Summary of operational stability of representative PSCs with dopant-free small-molecular HTMs.

HTM	Storage[a)]	RH (%)	T (℃)	Light source[b)]	MPP tracking[c)]	Ref.
2,7-BCz-OMeTAD	Amb, Unen	50	50	1-sun	71% after 150 h	[13]
FA-CN	Ar, Unen	\	45	UV filtered 1-sun	65% after 1300 h	[11]
TSHBC	Amb, Unen	45	\	1-sun	60% after 6.7 h	[14]
KR321	Ar, Unen	\	\	UV filtered 1-sun	60% after 650 h	[15]
Doped Spiro-OMeTAD	**Amb, En**	**35**	**30**	**MHL (1.1 sun)**	**10% after 1000 h** T_{80} **= 185 h**	**This work**
YZ18	**Amb, En**	**35**	**30**	**MHL (1.1 sun)**	**65% after 1000 h** T_{80} **= 717 h**	**This work**
YZ22	**Amb, En**	**35**	**30**	**MHL (1.1 sun)**	**81% after 1000 h** T_{80} **= 1617 h**	**This work**

a) Amb: ambient conditions; Ar: argon atmosphere; Unen: unencapsulated PSC; En: encapsulated PSC.
b) MHL: metal halide lamp.
c) T_{80} were extracted using the method described in **Figure S16**. Values of our cell parameters in this table are average values obtained from 5 devices studied under each condition.

Table S3. Summary of champion and average photovoltaic parameters of MAPbI PSCs under reverse voltage scan with doped Spiro-OMeTAD or YZ18 as HTM. Parameters followed by * are champion device parameters. Parameters in bracket are average parameters. Average and standard deviation values are from measuring 40 devices with each HTM.

HTM	J_{SC} (mA cm^{-2})	J_{SC} by EQE (mA cm^{-2})	V_{OC} (V)	FF	PCE (%)	PCE_{ST} (%)[a]
Doped Spiro-OMeTAD	21.5* (20.3 ± 0.6)	20.5*	1.01* (0.92 ± 0.03)	0.71* (0.68 ± 0.03)	15.4* (14.3 ± 0.5)	14.7*
YZ22	22.4* (21.1 ± 0.7)	21.3*	1.08* (1.00 ± 0.04)	0.75* (0.73 ± 0.02)	18.1* (16.9 ± 0.6)	17.6*

[a] Steady-state power-conversion efficiency at the maximum power point

Reference

1 Y. Zhang, S. G. Kim, D. K. Lee and N. G. Park, *ChemSusChem*, 2018, **11**, 1813–1823.

2 M. I. Saidaminov, M. A. Haque, J. Almutlaq, S. Sarmah, X. H. Miao, R. Begum, A. A. Zhumekenov, I. Dursun, N. Cho, B. Murali, O. F. Mohammed, T. Wu and O. M. Bakr, *Adv. Opt. Mater.*, 2017, **5**, 1600704.

3 M. V. Khenkin, E. A. Katz, A. Abate, G. Bardizza, J. J. Berry, C. Brabec, F. Brunetti, V. Bulović, Q. Burlingame, A. Di Carlo, R. Cheacharoen, Y.-B. Cheng, A. Colsmann, S. Cros, K. Domanski, M. Dusza, C. J. Fell, S. R. Forrest, Y. Galagan, D. Di Girolamo, M. Grätzel, A. Hagfeldt, E. von Hauff, H. Hoppe, J. Kettle, H. Köbler, M. S. Leite, S. Liu, Y.-L. Loo, J. M. Luther, C.-Q. Ma, M. Madsen, M. Manceau, M. Matheron, M. McGehee, R. Meitzner, M. K. Nazeeruddin, A. F. Nogueira, Ç. Odabaşı, A. Osherov, N.-G. Park, M. O. Reese, F. De Rossi, M. Saliba, U. S. Schubert, H. J. Snaith, S. D. Stranks, W. Tress, P. A. Troshin, V. Turkovic, S. Veenstra, I. Visoly-Fisher, A. Walsh, T. Watson, H. Xie, R. Yıldırım, S. M. Zakeeruddin, K. Zhu and M. Lira-Cantu, *Nat. Energy*, 2020, **5**, 35–49.

4 G. Tumen-Ulzii, C. Qin, D. Klotz, M. R. Leyden, P. Wang, M. Auffray, T. Fujihara, T. Matsushima, J. W. Lee, S. J. Lee, Y. Yang and C. Adachi, *Adv. Mater.*, 2020, **32**, 1905035.

5 S. Bai, P. Da, C. Li, Z. Wang, Z. Yuan, F. Fu, M. Kawecki, X. Liu, N. Sakai, J. T. W. Wang, S. Huettner, S. Buecheler, M. Fahlman, F. Gao and H. J. Snaith, *Nature*, 2019, **571**, 245–250.

6 X. Sun, Q. Xue, Z. Zhu, Q. Xiao, K. Jiang, H. L. Yip, H. Yan and Z. Li, *Chem. Sci.*, 2018, **9**, 2698–2704.

7 P. Xu, P. Liu, Y. Li, B. Xu, L. Kloo, L. Sun and Y. Hua, *ACS Appl. Mater. Interfaces*, 2018, **10**, 19697–19703.

8 J. Qiu, H. Liu, X. Li and S. Wang, *Chem. Eng. J.*, 2020, **387**, 123965.

9 J. Zhou, X. Yin, Z. Dong, A. Ali, Z. Song, N. Shrestha, S. S. Bista, Q. Bao, R. J. Ellingson, Y. Yan and W. Tang, *Angew. Chemie - Int. Ed.*, 2019, **58**, 13717–13721.

10 X. Yin, J. Zhou, Z. Song, Z. Dong, Q. Bao, N. Shrestha, S. S. Bista, R. J. Ellingson, Y. Yan and W. Tang, *Adv. Funct. Mater.*, 2019, **29**, 1904300.

11 S. Paek, P. Qin, Y. Lee, K. T. Cho, P. Gao, G. Grancini, E. Oveisi, P. Gratia, K. Rakstys, S. A. Al-Muhtaseb, C. Ludwig, J. Ko and M. K. Nazeeruddin, *Adv. Mater.*, 2017, **29**, 1606555.

12 C. Shen, Y. Wu, H. Zhang, E. Li, W. Zhang, X. Xu, W. Wu, H. Tian and W. H. Zhu, *Angew. Chemie - Int. Ed.*, 2019, **58**, 3784–3789.

13 C. Yin, J. Lu, Y. Xu, Y. Yun, K. Wang, J. Li, L. Jiang, J. Sun, A. D. Scully, F. Huang, J. Zhong, J. Wang, Y. B. Cheng, T. Qin and W. Huang, *Adv. Energy Mater.*, 2018, **8**, 1800538.

14 J. Cao, Y. M. Liu, X. Jing, J. Yin, J. Li, B. Xu, Y. Z. Tan and N. Zheng, *J. Am. Chem. Soc.*, 2015, **137**, 10914–10917.

15 K. Rakstys, S. Paek, P. Gao, P. Gratia, T. Marszalek, G. Grancini, K. T. Cho, K. Genevicius, V. Jankauskas, W. Pisula and M. K. Nazeeruddin, *J. Mater. Chem. A*, 2017, **5**, 7811–7815.